Arabian Journal of Chemistry (2023) **16**, 105177

King Saud University

Arabian Journal of Chemistry

www.ksu.edu.sa
www.sciencedirect.com

ORIGINAL ARTICLE

Nanostructured lipid carriers of ivabradine hydrochloride: Optimization, characterization and in-vivo estimation for management of stable angina

Roshan Kumar Dubey [a], Kamal Shah [b], Ahmad J. Obaidullah [c], Mohammed M. Alanazi [c], Hadil Faris Alotaibi [d], Hitesh Kumar Dewangan [e,*]

[a] *Department of Pharmaceutics, Mahatma Gandhi Institute of Pharmacy, Lucknow, Kanpur Rd, Junab Ganj, Uttar Pradesh 227101, India*
[b] *Institute of Pharmaceutical Research (IPR), GLA University, Mathura, NH-2 Mathura Delhi Road, PO- Chaumuhan, Mathura 281406, India*
[c] *Department of Pharmaceutical Chemistry, College of Pharmacy, King Saud University, P.O. Box 2457, Riyadh 11451, Saudi Arabia*
[d] *Department of Pharmaceutical Sciences, College of Pharmacy, Princess Nourah Bint AbdulRahman University, Riyadh 11671, Saudi Arabia*
[e] *University Institute of Pharma Sciences (UIPS), Chandigarh University, NH-95 Chandigarh Ludhiana Highway, Mohali, Punjab India*

Received 16 March 2023; accepted 15 July 2023
Available online 24 July 2023

KEYWORDS

Angina;
Ivabradine Hydrochloride (IBH-PNPs);
Nanostructured;
Lipid;
Carrier;
Formulation

Abstract Stable angina (angina pectoris) is a type of chest pain that happens when the heart muscle needs more oxygen than usual but it's not getting it at that moment because of heart disease. The drawback of the marketed formulation is required repeated administration of the drug due to low bioavailability. A recently licenced medication called ivabradine hydrochloride (IVB) is used to treat stable angina and signs of heart failure. Technical problems in the approved IBH tablets include a two-hour half-life, erratic systemic absorption, and a high rate of first-pass metabolism (> 50%). We therefore created a distinctive and cutting-edge formulation of IVB using a nano formulation approach like nanostructured lipid carriers (NLCs). The response surface method with a three-level Box–Behnken design was used for the creation and improvement of IVB. The optimized formulation was proceeded for physicochemical characterizations like particle size, zeta potential, morphology (TEM and SEM), entrapment efficiency, in-vitro release, stability studies, compatibility study (DSC, FTIR and XRD), hemocompatibility study, ex-vivo permeability, and in-vivo ang-

* Corresponding author.
E-mail address: hiteshdewangan.hd@gmail.com (H. Kumar Dewangan).
Peer review under responsibility of King Saud University. Production and hosting by Elsevier.

Production and hosting by Elsevier

https://doi.org/10.1016/j.arabjc.2023.105177

ina study. As results, optimized formulation was found to be 114.45 ± 5.14 nm particle size with 83.45 ± 3.23% entrapment efficiency and biphasic release. The formulation showed spherical and compatible with excipients, no interaction was observed and hemocompatible. The IBH-NLCss showed more permeability (1.85 folds) as compared to the marketed dosage form. The in-vivo pharmacological activity was established in terms of decrease in severity and duration of ST-segment depression in vasopressin-induced angina model in experimental rats.

1. Introduction

The escalating mortality and morbidity rates, coronary heart disease (CHD) are global concern. CHD-related mortality and impairments are steadily increasing in underdeveloped countries, while falling in developed countries. South Asia has one of the highest CHD mortality rates in the world, according to the World Health Organization (WHO). One of the consequences of CHD is stable angina, which causes chest discomfort and agony. It occurs when the cardiac muscles do not receive adequate blood supply due to narrowing or blockage of one or more blood vessels. Angina affects the neck, jaw, shoulder, back, and arm, causing pain and discomfort (Sharma et al. 2019).

A unique drug called Iabradine hydrochloride (IVB) is used to treat the symptoms of stable angina pectoris. IVB works by diminishing the pace of heartbeat in an alternate machine for beta blockers and calcium blockers, the mainly two regularly recommended anginal medications named as cardiotonic operator. Plasma Half-life is around 2 hrs, and bioavailability is 40% (Alagusundaram et al. 2009; Dewangan et al. 2020). Conveyance frameworks use lipid-actuated lipid segments as promising bearers are increasing expanding consideration nowadays in light of their capacity to build dissolvability (Dewangan, 2021) and water and/or lipophilic drying reduce dynamic compounds' bioavailability (Braidy et al. 2017; Onoue et al. 2011; O'Driscoll et al. 2008). NLCs are second-age lipids nanoparticles separated from SLNs as were depicted (Mishra et al. 2023b; Müller et al. 2002). The NLCs have points of interest related with SLNs, obviously, for example, the event of hydrophobic and hydrophilic revisions PCs and the intensity of controlled transmission too Free stockpiling highlights above free state. Furthermore, NLCs can shield PCs from mechanical, physical, oxidative, or light-reflecting; sink extremely low danger; and furthermore, requiring little to no effort (Joshi and Müller, 2009; Müller et al. 2007). The nanoformulations SLNs and NLCs derived from oil emulsions were used to plan a fluid lipid with a robust lipid network.

Now, this work was aimed to prepare Nanostructured Lipid Carriers (NLCs) of Ivabradine Hydrochloride (IBH-NLCs) by emulsification method; using Design-Expert Software®. The 3-level, 3-factor Box-Behnken experimental design was utilized for the understanding of the effect of independent process variables and formulation variables on dependent variables. Further, the optimized IBH-NLCs was characterized for various physicochemical properties like particle size, zeta potential, morphology, *in-vitro* studies, interaction study, stability studies, hemocompatibility, *ex-vivo* intestinal permeation study, and *in-vivo* anti-anginal activity in Wistar rats.

2. Materials

Ivabradine Hydrochloride (IVB) was supplied by Yellow Chem Pharma Products, Mumbai. Ingredient such as Lecithin (containing 90% soybean phosphatidylcholine), Poloxamer 188 (Pluronic F68), Methanol and acetonitrile was supplied by Central Drug House, Ltd. New Delhi, India. All chemicals used in this experiment were analytical grade and having specificity.

3. Methodology

IVB-NLCs was set up by liquefy emulsification method and high-pressure homogenesis at room temperature (25–30 °C) (Dewangan et al. 2018). Quickly, 3 mL of ethanol was added to the lipid stage as a covalent, which is indistinguishable with IVB, strong lipids, fluid lipids, and lecithin. In a water bath, including the surfactant and lipid stages, was warmed to 75 ^{0}C., Than water phase containing emulsifier was added slowly. The lipid grid was brought into the watery network, and the blending step was mixed for 10 min at 500 rpm and afterward proceeded for high-shear homogenizer (SRH-S300) for 2 min at 1000 rpm. Further, the coarse emulsion was homogenized utilizing a nano homogenizer machine AH100D under 800 bars for 10 cycles. At long last, the subsequent nano emulsion was permitted to frame IVB - NLCs to cool to room temperature.

Using Design-Expert Software® 7.0.0, the NLCs were optimised using the Response Surface Methodology (RSM), which also applied a 3-level, 2-factor, Box-Behnken experimental design and established a link between independent and dependent variables. The emulsifier to lipid ratio (X1), lecithin to Poloxamer-188 ratio (X2), and liquid lipid to solid liquid ratio (X3) were identified as key variables based on preliminary tests. These variables were presented in Table 1 at three levels: −1 (low), 0 (medium), +1 (high).

3.1. Design optimisation of IVB-NLCs by Box–Behnken

A 17 formulation design with three-dimensional feature levels, were carried out in the current study using a response mechanism (RSM) based on BBD. Currently, response patterns are identified using Design 8.0.5 Software (Stat-Ease Inc., Min-

Table 1 Variables with respective coded levels of the Box–Behnken design for the preparation and optimization of IVB - NLCs.

Variable			
Independent variable	Levels		
	Low (-1)	Medium (0)	High (+1)
X_1: emulsifier to lipid ratio	1	1.75	2.5
X_2: lecithin to Poloxamer-188 ratio	0.5	1.25	2
X_3: liquid lipid to solid liquid ratio	0.33	1	1.67
Dependent variable Constraints			
Y_1: mean particle size (nm)	Minimum		
Y_2: encapsulation efficiency (%)	Maximum		

neapolis, USA), which is followed by the development of the models displayed below:

$$Y = \lambda_0 + \lambda_1 X_1 + \lambda_2 X_2 + \lambda_3 X_3 + \lambda_1^2 X_1 X_2 + \lambda_{13} X_1 X_3 + \lambda_{23} X_2 X_3 + \lambda_{11} X_1^2 + \lambda_{22} X_2^2 + \lambda_{33} X_3^2 \quad (1)$$

The measured responses (Y) were positive particle size (Y1) and EE (Y2), as indicated in (1). Emulsifier-to-lipid ratio (X1), lecithin-to-Polaxer 188 ratio (X2), and lipid-to-solid lipid ratio (X3) were the three independent variables that were selected (Ngan et al. 2014). The high, medium, and low levels for each factor are denoted by the symbols 1, 0, and −1, respectively (Table 1). λ_0 is line; λ_1, λ_2, and λ_3 are consecutive points; λ_{12}, λ_{13}, and λ_{23} are coordinates; and λ_{11}, λ_{22}, and λ_{33} is the quadratic coefficients.

3.2. Physicochemical characterization

3.2.1. Particle size and zeta potential

A Delsa-Nano C particle size analyser was used to measure the particle size and PDI of prepared IBH-PNPs (Beckman Coulter, UK), which uses photon correlation spectroscopy as its basis. The observations were carried out utilising scattering light generated by a typical He-Ne laser at a fixed angle of 165^0 at a temperature of 25 ^{0}C. In order to calculate, the electrophoretic mobility of charged particles under the influence of an applied electric field was measured from the zeta potential of IBH-PNPs. Before all measurements, IBH-NLCs were diluted and sonicated.

3.2.2. Estimation of entrapment efficiency (EE)

Entrapment efficiency of IVB-NLCs are controlled via estimating free IVB in the water stage, detached utilizing centrifugation (Sun et al. 2014). 500 µL IVB-NLCs was added to the centrifugal filter Unit 100 kDa (Millipore Co, USA) and uses a UniCen MR (Herolab, Germany) to radiate for 20 min at 40°Celsius at 3000 rpm (Lakshmi et al. 2018). In order to analyse the filtrate, HPLC was used with a Dionex UltiMate 3000 (Sunnyvale, USA) by way of the C8 segment. The filtrate was degraded in methanol. A portable stage or mobile phase made of distilled water and acetonitrile (55:45 v/v) was used for the chromatographic analysis, which was carried out at 300C and 284 nm. The infusion volume was 20 L, and the stream speed was 1.0 mL/min. The 0.22 m membrane is used to describe the ultrapure water at the front. Using a set of criteria, the EE channel was identified (Mishra et al. 2023a):

$$EE(\%) = \frac{W_{total} - W_{free}}{W_{total}} \times 100 \quad (2)$$

Where w_{total} is quantity of initial IVB used and w_{free} is quantity of free IVB in the aqueous phase.

3.2.3. Morphology by TEM and SEM

In Transmission Electron Microscopy (TEM, JEM-2100F electron microscope, JEOL Ltd., Tokyo, Japan) at 200 kV, the morphological IVB-NLC traits were observed. The samples were dropped onto a copper grid made of Formvar/Carbon with a 230 mesh size, air-dried for 24 h at normal temperature, and then negatively saturated with phosphotungstic acid (1% w/v) about 25 min before examine.

For Scanning Electron Microscopy (SEM: Zeiss, Evo Research Ltd., Tokyo, Japan), a small drop of the nanoformulation was applied to the glass stub and allowed to air dry to found the thin film. After the dried coated with gold using a glass sputter coater in a high vacuum evaporator and then observed in SEM microscope.

3.2.4. In-vitro IVB release estimation

Employment of dialysis membrane technique, for activation of membrane it was placed over night in the phosphate buffer solution. IVB-NLCs (5 mL) filled in the dialysis membrane and it was kept in the phosphate buffer (150 mL, pH 7.4), stirred at (100 rpm at 37 ± 5 ^{0}C). At a time up to 72 hrs, interval sampling was done and maintain the sink condition. HPLC, at 284 nm, was used to analyse samples. All experiment was performed in the triplicate manner.

3.2.5. Interaction study by DSC and FTIR

The IVB-NLCs and IVB were analysed by Differential Scanning Calorimetry (DSC Q20, thermograms (TA Instruments, New Castle, USA). The temperature raised from 25 to 240 °C during the temperature or cooling scan of 10 °C min^{-1} when 3 mg of samples were placed in normalised aluminium pans. Dry nitrogen was employed as a liquid gas during the hot scales, and a reference for analysis was an empty pan (Dewangan et al. 2021; Ahmadian-Fard-Fini et al., 2021).

The Fourier transform infrared spectroscopy (FTIR: SHIMADZU 8400, Japan) was also used to determine compatibility. The characteristic bands and peaks of poloxamer, lecithin, IBH, physical mixture, and IBH-NLCs were examined in order to comprehend the interaction (Ahmadian-Fard-Fini et al., 2019; Ahmadian-Fard-Fini et al., 2020). The samples were thinly compressed with potassium bromide (KBr) using a pressed pellet method. The pellets were next exposed to the IR path length for scanning against a KBr background that was left empty. The scanning area was between 400 and 4,000 cm^{-1}.

3.2.6. X-ray severity scales

It was decided to gather and compare XRD data using lyophilized IVB-NLCs, lyophilized blank NLCs, and IVB using the X-ray diffractometer X'SPert3Power (PANalytical B.V., Almelo, Netherlands). Under CuK radiation, 40 kV of voltage, and 40 mA of current, an XRD examination was conducted (step size: 0.013; scan step time: 8.67 s) over an angle size of variation of 0 to 2 to 90 (Deepika et al. 2019).

3.3. Storage stability

Due to their propensity to aggregate due to their enormous surface area, nanoparticles eventually grow larger in size. Show the following physical characteristics if the formulation was unstable: colour, odour, taste, and texture. The optimised IVB-NLCs stability investigations were conducted at normal temperature (25 ^{0}C and 60 %RH) and in a refrigerator (2 ^{0}C).

3.4. Hemocompatibility study

3.4.1. Evaluation of hemolysis

Evaluation of hemolysis is required to demonstrate heme compatibility when NLCs are reached in circulation. Placebo-

NLCs, IVB and IVB loaded NLCs have been performed using reported methods (Dewangan et al. 2018; Hung et al. 2004). In short, human blood was obtained from an authorized blood bank. The blood plasma membrane is carefully decomposed, mixed in an equal volume and gently mixed with normal saline solution. Small volumes of cell suspension (5 mL) were centrifuged at 1344 × g for 10 min in a clean graduate centrifuge tube at room temperature. Erythrocyte suspension was then centrifuged. The same process for washing was thrice. Finally, the solution is dilute to 50 mL and resuspended in regular saline solution (Dewangan et al. 2022).

Samples such as placebo IVB, and IVB loaded NLCs (equivalent to 10 and 20 ng/mL of IVB), placebo-nanoparticles (equal to volume of IVB loaded nanoparticles) were mixed with erythrocyte suspension (2 mL) in sterile tubes. As positive controls, 100% of the erythrocytes were lysed; as spontaneous negative controls, samples of normal saline and erythrocyte suspension were diluted with 1% Triton X-100, respectively. Every 15 min, the samples were gently mixed while being incubated at 37oC. At 0.5, 1, 2, 4, and 8 h, aliquots (200 L) were collected and centrifuged at 1344 g for 10 min. Thereafter, 100 L of the supernatant was oxidised to haemoglobin for 30 min at room temperature. to oxymoglobin after oxidation. The absorbance was measured spectrophotometrically at 284 nm (Synergy H1 Hybrid, Biotech, USA). The following formula is used to determine the proportion of hemolysis:

$$\%Haemolysis = \frac{A_{Sample} - A_{SpontaneuousControl}}{A_{PositiveControl}} \times 100$$

Where A_{sample} is the absorbance of the erythrocyte supernatant after being incubated with IVB loaded NLCs formulations, $A_{Spontaneous\ Control}$ is the absorbance of the erythrocyte supernatant after being incubated with normal saline equivalent to the volume of the samples, and $A_{Positive\ Control}$ is the absorbance of the erythrocyte supernatant after being incubated with 1% triton X-100 solution. The data is shown as mean ± SD (n = 3) and experiments were carried out in triplicate.

3.4.2. Qualitative platelet aggregation

Peripheral blood smears were microscopically evaluated after whole blood is incubated with test specimens (10 and 20 ng/mL of plain IVB, IVB loaded NLCs and placebo-NLCs). After the peripheral blood smears were incubated, the samples were prepared, spread on a clean glass slide, and then air dried after 5 min of Leishman stain (Span Diagnostics, India). After washing the slides, the cover glass was placed on it, analysed with an optical microscope for immersion, and images were taken using a digital camera.

3.4.3. In-vivo study

In propylene cages male wister rates (200–250 g) were placed and kept in 12 h light/dark cycle run for the stabilization of standard laboratory atmosphere. All experiment was under the guidelines of CPCSEA (Committee for the Purpose of Control and Supervision of Experiments on Animals). The animals were sacrificed by Euthanasia; disposal by incineration.

3.4.4. Ex-vivo intestinal permeation study

Intestinal permeation potential of IVB-NLCs across GIT was evaluated by non-everted gut sac technique (Singh et al. 2010). The experimental rat was divided into two groups (=3) and following the ether anaesthesia that the cervical dislocation sacrificed. A cold saline solution is placed immediately after the small intestine is split in the stomach. A body saline solution was then administered using a syringe to remove any intestinal contents and cut components from a 20–30 cm section of small intestine that had been separated from the pyloric sphincter. Using a laboratory aerator and a solution of IVB and IVB-NLCs, constant aeration (carbogen, 95:5 O_2/CO_2) was applied to the intestines at a temperature of 5 °C. Samples were taken periodically from the receptor chamber and repeated with an identical volume of warm, fresh water in front of the solution. The withdrawal sample was sonicated for 15 min before being filtered using 0.2-m membrane filters. After the suitable dilution analysed in UV at 284 nm (Lakshmi et al. 2022; Gandhi et al. 2014). Using the formula below, IBH solution and IBH-PNPs' apparent permeability coefficients (Papp) were calculated and expressed in cm/s. The formula was used to get the Permeability Enhancement Ratio for IVB.

$$P_{app} = \partial Q/\partial t * 1/AC_0$$

Where A is the exposed intestinal tissue surface area (cm^2), $\partial Q/\partial t$ is the steady-state appearance rate of IVB-NLC in the receiver compartment, and Co is the initial concentration of the IVB in the donor compartment at zero time.

3.4.5. In-vivo anti-anginal single-dose study

The experimental rat was divided into 4 groups; normal control, disease control, test and marketed formulation. In each groups contain 6 rats. Calculated equivalent dose 1.54 mg/kg for test and marketed formulation as per dose conversion formula. After the 1 h induce the angina and the dose was 2 mL orally administered by gavage tube to all groups.

3.4.6. Induction of myocardial ischemia measurement of ST-segment depression

The experimental male rats Inhalation anaesthesia (Isoflurane) used to anesthetize the experimental male rats and placed on a heating pad to maintain a temperature 37 °C. During these study for maintenance of aesthesia given 0.2 L/min was used, which is the mixture of 2% of isoflurane in 100% oxygen. Vasopressin was given IV after the stabilization of aesthesia with the dose 2 IU/kg (Hirata et al. 2005; Ikeda et al. 2006). 2 mL IVB-NLC or dispersed IVB tablet in purified water was given after the 1 h. The cited ischemia generation was used for three consecutive days. Vasopressin was administered intravenously, and Lab Scribe software used the ST-segment depression as a measure of myocardial ischemia.

4. Results and discussion

4.1. Optimisation of IVB-NLCs

The Table 2 represented the 17 various approaches that were created based on the BBD's design to determine which of the most sensitive types are independent. Lipid-to-solid lipid ratio

(X3), ratio of lecithin-to-Poloxamer 188 (X2), and ratio of emulsifier-to-lipid ratio (X1) are the variables that have the biggest effects on the characteristics of IVB-NLCs. Analysis of variance was used to statistically confirm lifetime evaluations, and Table 3 summarises the outcomes of the regression study. The effects of the independent factors on the observed particle size distributions are shown on 3D graphs of the response surface, and the EE is displayed in Figs. 1 and 2.

4.1.1. Effect on mean particle size

As indicated in Table 2, the mean particle size (Y1) ranged from 95.21 nm (Formulation 7) to 189.05 nm (Formulation 9). The quadratic equation has been used to illustrate how independent variables affect mean particle size as follows:

$$\begin{aligned} Y_1 = {} & -25.59823 + 209.73428^{*} X_1 + 7.38682^{*} X_2 \\ & + 3.33748 * X_3 - 41.52444 * X_1 * X_2 - 5.52239 * X_1 * X_3 \\ & + 14.36318 * X_2 * X_3 - 42.12800 * X_1{}^2 \\ & + 16.88978 * X_2{}^2 - 22.68211 * X_3{}^2 \ldots\ldots \end{aligned} \quad (3)$$

The negative incentive preceding the variable in the quadratic condition showed that condition (3) exposed negative impact on factors X1, X2, and X3 on Y1. A larger

Table 2 Preparation and optimization of IVB-NLCs formulations using Box–Behnken Design Optimization.

Formulation	Independent variables			Dependent variables			
				Observed value		Predicted value	
	X_1	X_2	X_3	Y_1	Y_2	Y_1	Y_2
1	1	0.5	1	120.25 ± 4.26	80.56 ± 4.91	180.87	79.84
2	2.5	0.5	1	164.65 ± 2.46	65.58 ± 5.50	180.63	79.89
3	1	2	1	145.98 ± 9.45	88.25 ± 3.98	180.13	80.01
4	2.5	2	1	96.95 ± 4.23	79.46 ± 2.54	183.33	79.26
5	1	1.25	0.33	114.45 ± 5.14	83.45 ± 3.23	112.15	86.04
6	2.5	1.25	0.33	134.89 ± 5.56	84.16 ± 6.48	186.36	78.54
7	1	1.25	1.67	95.21 ± 6.10	73.66 ± 7.23	187.17	78.34
8	2.5	1.25	1.67	106.55 ± 6.61	86.55 ± 3.56	188.18	78.09
9	1.75	0.5	0.33	189.05 ± 9.42	81.05 ± 9.41	171.50	82.01
10	1.75	2	0.33	169.52 ± 2.35	76.65 ± 9.01	182.39	79.01
11	1.75	0.5	1.67	106.99 ± 3.48	77.65 ± 5.43	187.89	77.82
12	1.75	2	1.67	116.33 ± 6.02	80.92 ± 9.31	176.56	80.20
13	1.75	1.25	1	136.92 ± 32	84.48 ± 3.08	189.05	77.46
14	1.75	1.25	1	100.62 ± 3.10	59.95 ± 4.66	187.53	77.50
15	1.75	1.25	1	173.39 ± 78	60.25 ± 8.22	151.07	88.24
16	1.75	1.25	1	167.62 ± 2.07	80.81 ± 9.08	183.57	77.76
17	1.75	1.25	1	152.22 ± 5.38	73.06 ± 6.91	150.76	78.63

X_1 = emulsifier-to-lipid ratio, X_2 = lecithin-to-Poloxamer 188 ratio, X_3 = liquid lipid-to-solid liquid ratio, Y_1 = mean particle size (nm), and Y_2 = encapsulation efficiency (%).

Table 3 Statistical analysis results of lack of fit test and model summary for mean particle size.

Source	Sum of square	df	Mean square	F-value	P-value
Model	10116.96	9	1124.11	1.67	0.2559
X_1	106.22	1	106.22	0.16	0.7031
X_2	340.08	1	340.08	0.51	0.5003
X_3	4087.44	1	4087.44	6.07	0.0432
X_1X_2	2182.29	1	2182.29	3.24	0.1148
X_1X_3	30.80	1	30.80	0.046	0.8367
X_2X_3	208.37	1	208.37	0.31	0.5954
X_1^2	2364.41	1	2364.41	3.51	0.1031
X_2^2	380.04	1	380.04	0.56	0.4770
X_3^2	436.52	1	436.52	0.65	0.4472
Residual	4713.75	7	673.39		
Lack of fit	1315.75	3	438.58	0.52	0.6931
Pure Error	3396.00	4	849.50		
Cor Total	14830.71	16			
Std. Dev.	25.95				
Mean	134.68				
C.V. %	19.27				
R^2	0.6822				
Adj R^2	0.2735				
Adeq Precision	4.673				

emulsifier-to-lipid percentage may encourage the formation of smaller particles and enable higher adjustability of nano framework due to the reduction in interfacial strain between the lipid grid and the hydrophilic stage. Fig. 1(a)–1 show the 3D surface plots showing the effect of association between X1 and X2, X1–X3, and X2-X3 on molecule size (c). The fluid lipid-to-strong lipid proportion (X3 and X32), in particular, has a notable impact on the mean molecule size of IVB-NLC, as shown in Table 3. The low value demonstrated that the observed characteristics matched those that were predicted, and connection coefficient (R2) was 0.6822 with a 19.27% coefficient of variation. "Adeq Precision" (Raghuvanshi et al. 2022) estimated that the model's sign-to-commotion ratio was 4.673 (> 4), indicating that it was adequate for the typical molecule size (Ye et al. 2016).

4.1.2. Impact on entrapment efficiency

The value for EE with the selected levels of variables ranged from 59.95% (Formulation 14) to 88.25% (Formulation 3), with an average value of 76.30%. The quadratic formula below demonstrated how different independent factors affected EE:

$$Y_2 = +142.60603 - 45.51057 * X_1 - 12.14592 * X_2 - 45.60525 * X_3 + 2.75111 * X_1 * X_2 + 7.55224 * X_1 * X_3 + 3.81592 * X_2 * X_3 + 9.23556 * X_1^2 + 2.76889 * X_2^2 + 12.92047 * X_3^2 \quad (4)$$

Moreover, the terms X1-X2 and X2-X3 had negative effects on particle size, whereas X1-X3 had beneficial effects on the EE of IVB-NLC (Pradhan et al. 2015). Fig. 2(a)-2 show the

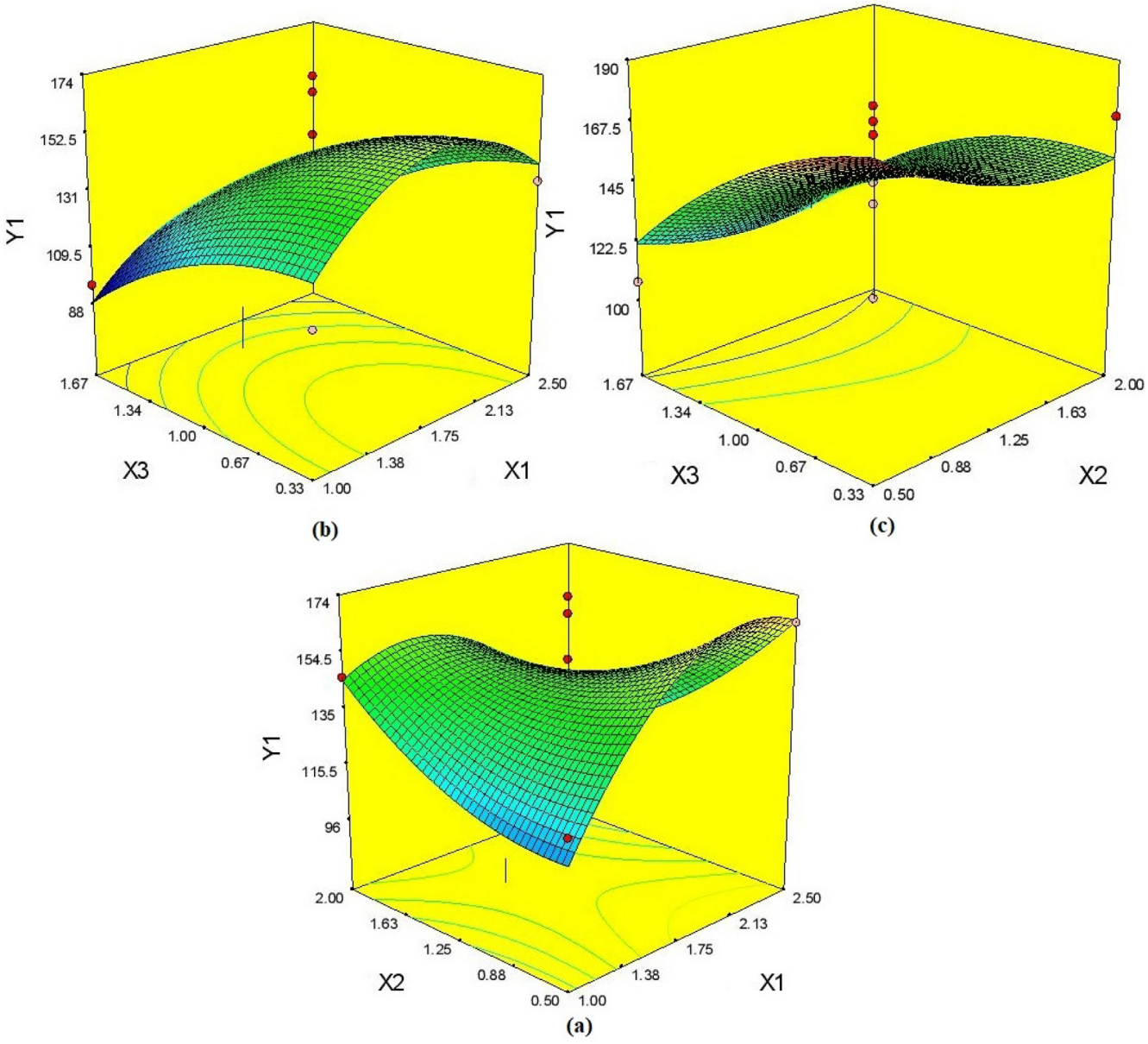

Fig. 1 3D response surface plot for the effect of emulsifier-to-lipid ratio (X_1), lecithin-to Poloxamer 188 ratio (X_2) and liquid lipid-to-solid liquid ratio (X_3) on mean particle size of IVB-NLC. (a) Effect of X_1- X_2 interaction terms; (b) effect of X_1- X_3 interaction terms; (c) effect of X_2- X_3 interaction terms.

3D response surface graphs that depict how X1-X2, X1-X3, and X2-X3 interact to affect EE (c). The model's importance for EE was suggested by the F-value of 0.48. There was a strong correlation between predicted and experimental values, as indicated by the low values of the coefficient of variation (13.27%) and the coefficient of correlation (R2 = 0.3798).

4.1.3. Optimization and validation

Based on requirements of satisfying minimum mean particle size and maximising value of EE produced via Design Expert software, optimization of IVB-NLCs preparation was selected. Lecithin to Poloxamer 188 ratio and, liquid lipid to solid lipid ratio were selected as 1.35 and 0.95, and emulsifier to lipid ratio of 1.76 were chosen as the optimised compositions, which were advised to achieve fundamentals of optimised IVB-NLCs formulation. The mean particle size and EE for this chosen batch were determined to be 114. 45 ± 5.14 nm and 83.45 ± 3.23 nm, respectively, while the anticipated values of 112.15 nm and 86.04%, produced by Design Expert programme, were establish to be in good arrangement (Yadav et al. 2022). The optimized batch zeta potential was found to be −21.3 mV.

4.2. Morphology study

Optimized batch was found to be spheroidal in shape, well segregated, and monodisperse indicating that nanoformulation is quite stable. TEM images of IVB-NLCs presented in Fig. 3(A) which showed spherical and uniform in size. It has been discovered that the real size determined by TEM is smaller than

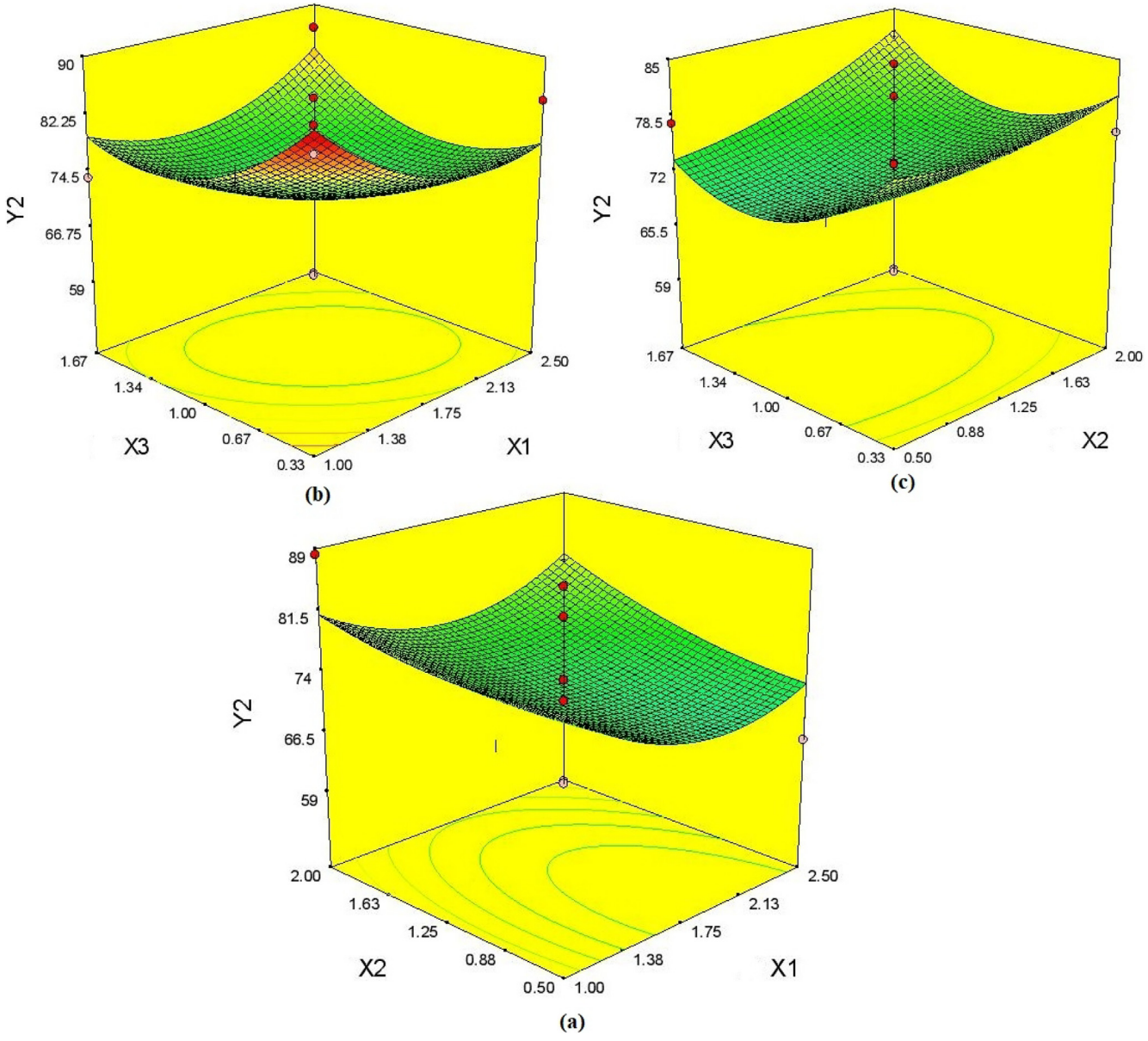

Fig. 2 3D response surface plot for the effect of emulsifier-to-lipid ratio (X_1), lecithin-to Poloxamer 188 ratio (X_2) and liquid lipid-to-solid liquid ratio (X_3) entrapment efficiency of IVB-NLC. (a) Effect of X_1- X_2 interaction terms; (b) effect of X_1- X_3 interaction terms; (c) effect of X_2- X_3 interaction terms.

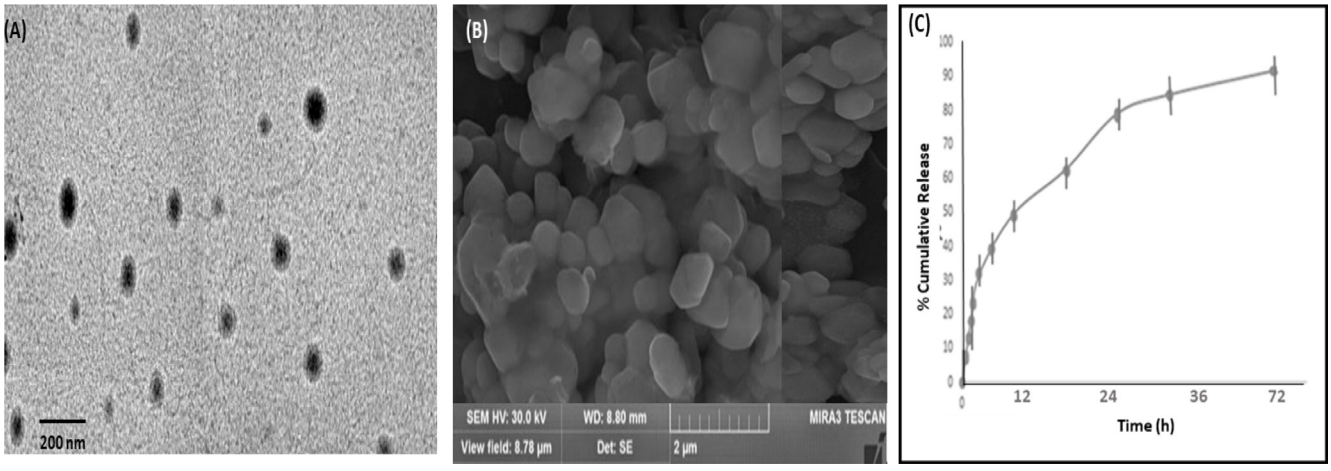

Fig. 3 Microscopic image (A) TEM photomicrographs of IVB-NLCs, scale bar represents at 200 nm (B) SEM image of IVB-NLCs (C). In-vitro drug release profile of IVB-NLCs.

the hydrodynamic size determined by DLS. The solvent layer that is linked to the particle is recalled in DLS as one example of the differences that are thought to exist (Singh et al. 2016, Sharma et al. 2022). In SEM image (Fig. 3(B)) showed onodispersed particles, indicated that enough surface charge is present on the surface of nanoparticles which is keeping them apart. It was further supported by negative zeta potential value (see Table 4).

4.3. In-vitro drug release study

In the Fig. 3(C) slow release of IVB nanoparticle in PBS, pH 7.4 for 72 h. The release data of the optimised formulation around 85.46% and burst release around 28.12% in 1 h. Slow release of drug after the burst release, which show the constant drug diffusivity through polymer erosion. The IVB is incorporated inside the lipid membrane, which is act like a double layer plasma membrane, so the release is very slow. According to the release pattern, it showed the good and prolong release of drug.

4.4. Interaction study

Fig. 4(A) Solid state characterisation (DSC), depicts a pronounced endothermic peak that coincided with the melting point of the IVB at 194 °C. In formation of IVB-NLCs, melting of IVB was unknown detection, which can be reported as being present IVB is in an amorphous or scattered state of muscle change within lipid matrix or a small part of IVB were available for IVB-NLCs as an alternative to crystalline state, very small IVB loading in IVB-NLCs would render inaccessible soluble event of any fraction using DSC-based techniques (Yadav et al. 2022). This practice can also be called disruption of NOBs and survivors in IVB-NLC crystallisation. Moreover, the Gibbs-Thomson equation states that particle size and has discernible impact on how lipid particles' endotherms dissolve in the nanoscale range.

The FT-IR spectra of the IVB revealed characteristic bands at, 1209 cm^{-1} (ether), 1460 cm^{-1} (C = C) (Shar), 1647 cm^{-1} (carbonyl), 2833 cm^{-1} (methyl) 3414 cm^{-1} (amine). The spec-

Table 4 Statistical analysis results of lack of fit test and model summary for entrapment efficiency.

Source	Sum of square	df	Mean square	F-value	P-value
Model	456.44	9	50.72	0.48	0.8515
X_1	21.68	1	21.68	0.20	0.6654
X_2	52.22	1	52.22	0.49	0.5063
X_3	11.35	1	11.35	0.11	0.7536
X_1X_2	9.58	1	9.58	0.090	0.7729
X_1X_3	57.61	1	57.61	0.54	0.4859
X_2X_3	14.71	1	14.71	0.14	0.7211
X_1^2	113.63	1	113.63	1.07	0.3359
X_2^2	10.21	1	10.21	0.096	0.7658
X_3^2	141.64	1	141.64	1.33	0.2866
Residual	745.28	7	106.47		
Lack of fit	227.95	3	75.98	0.59	0.6547
Pure Error		517.33	4	129.33	
Cor Total		1201.73	16		
Std. Dev.	10.32				
R^2	0.3798				
Mean	77.62				
C.V. %	13.29				
Adeq Precision	2.227				

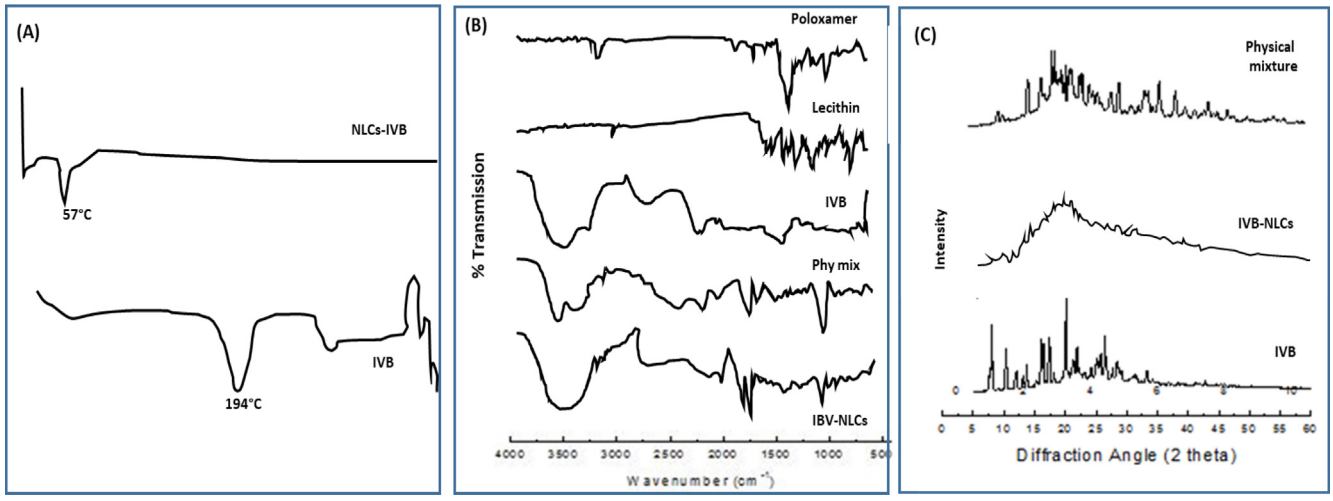

Fig. 4 (A) DSC thermogram of drug IVB and IVB-NLCs (B) FTIR spectra of poloxamer, lecithin, drug IVB, physical mixture and IVB-NLCs. (C) X-ray Diffractograms of drug IVB, IVB-NLCs and physical mixture.

tra of physical mixture and lyophilized IBH-NLCs revealed bands at 3420 cm^{-1}, 1206 cm^{-1}, 2845 cm^{-1}, 1645 cm^{-1}, and 1450 cm^{-1}. Fig. 4(B)'s overlay FTIR spectrum of the optimised formulation illustrates the lack of any drug-excipient interactions. The drug is preserved in its original form and there is no chemical interaction, according to the absorption bands of the drug present in formulation spectra (Ahmadian-Fard-Fini et al., 2018).

4.5. Solid state characterisation (XRD)

IVB XRD spectra show in Fig. 4(C), showed different peaks at intensity 2θ, which shows large crystalline structure of IVB (e.g., three sharp peaks in $2\theta = 7.61^{o}$, 11.46^{o}, and 11.86^{o}; Five midsummer peaks and two-fold peaks in low power occur at 5.97^{o}, 9.64^{o}, and 13.42^{o}. The slighty presence of IVB peaks from the IVB-NLCs XRD patterns indicated that the IVB molecule had lost its crystal structure and had instead joined up with the matrix of the NLCs to form an amorphous complex. These results are connected to the DSC analysis's findings, which show that IVB changed from being crystalline to amorphous over time. A crystalline solid can be bombarded by high-kinetic-energy ions to change it into an amorphous solid. Amorphous phases can form when crystalline layers undergo interdiffusion, or atomic-scale mixing, under specific composition and temperature circumstances. (Karami et al., 2021; Orooji et al., 2020; Kavousi et al., 2019).

4.6. Storage stability study

During the stability study no significant changes was observed at the mentioned environmental conditions (Table 5). Some deposition was observed in the base of the container and it was resolved by the normal shaking. IVB-entrapment NLCs effectiveness and particle size changed insignificantly.

4.7. Hemocompatibility studies

4.7.1. Evaluation of hemolysis

Hemolytic evaluation is needed to prove safety. Comparative hemolysis results of placebo-NLCs, plane IVB and IVB nanoparticles, at concentrations of 10 and 20 ng/mL, respectively. IVB nanoparticles showed an equivalent hemolysis value of 1% over the study period (8 h). The hemolysis of 10 ng/L equivalent placebo-nanoparticles was found to be statistically similar to that of IVB nanoparticles. Similarly, at an equivalent volume of 20 ng / mL, placebo-nanoparticles showed significantly higher hemolysis values at 8 h compared with IVB nanoparticles. The hemolysis values of placebo-nanoparticles were found to be significantly higher at 4 and 8 h compared with IVB nanoparticles at an equivalent volume of 30 ng/mL. Although IVB nanoparticles contain all components of placebo-nanoparticles, IVB-loaded nanoparticles show significantly less hemolysis at some points in the same concentrations of 10 and 20 ng / mL over time. Furthermore, IVB nanoparticles at multiple time points of three equivalent

Table 5 Storage Stability study results of IVB-NLC at room temperature and refrigerated conditions.

Condition	Room Temperature				Refrigerated condition			
Days	**0**	**30**	**6**	**90**	**0**	**30**	**60**	**90**
Particle size	120.25 ± 4.26	126.34 ± 2.05	130.06 ± 3.24	138.09 ± 6.02	120.25 ± 4.26	124.62 ± 6.11	128.88 ± 2.36	135.69 ± 2.05
%EE	80.56 ± 4.91	75.05 ± 3.02	69.68 ± 5.31	65.06 ± 3.12	80.56 ± 4.91	76.89 ± 3.05	71.25 ± 4.23	68.06 ± 2.15

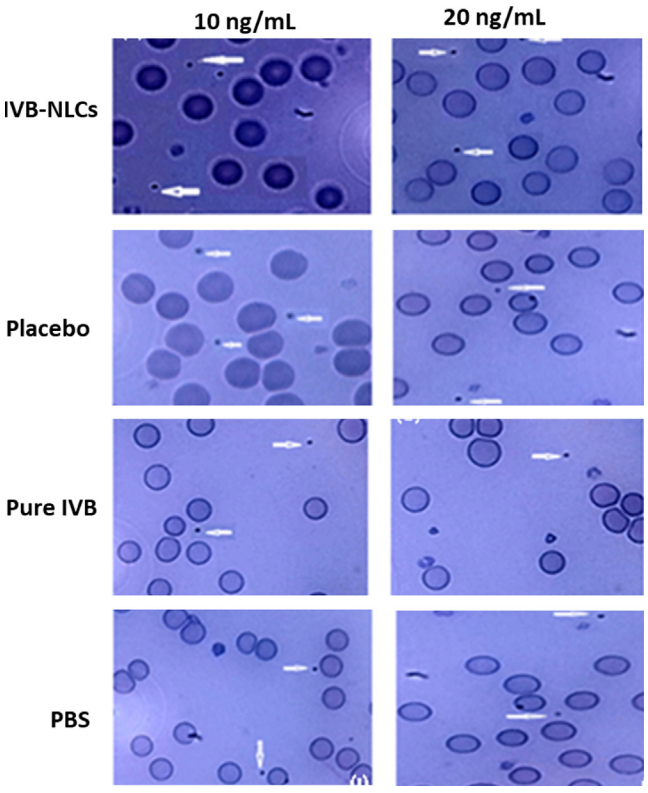

Fig. 5 Light microscopy images (100X resolution) of Leishman's stained whole blood samples after treating with PBS, pure IVB, placebo and IVB-NLCs, in concentration of 10 and 20 ng/mL.

versions showed lower hemolysis values than nanoparticles and placebo-nanoparticles.

4.7.2. Qualitative platelet aggregation

Total IVB, IVB nanoparticles (equivalent to 10 and 20 ng/mL of IVB), placebo-nanoparticles (equal to volume of IVB nanoparticles) were analyzed by total microscope by plane microscope. Erythrocytes, white blood cells and the platelets were seen under a microscope. and imaging cap. Aggregation of platelet aggregation was not observed at three different concentrations of the test samples (Fig. 5). Platelets were distributed on whole blood smears on microscopic examination of all test specimens. Observations indicate that IVB nanoparticles are nontoxic and hem compatible in nature.

4.8. Animal studies

4.8.1. Ex-vivo intestinal permeation study

Higher permeation of IVB-NLCs as compared to the IVB solution due to the large surface area (Fig. 6: A and B). 0.28 26 ± 0.023 × 10^{-5} and 0.5253 ± 0.036 × 10^{-5} cm/s, the permeability coefficients for IVB solution and IVB-NLCs respectively.

4.8.2. In-vivo anti-anginal activity

Impact of Ivabradine Hydrochloride on ST-Segment depression time, duration, and onset: As compared to disease Control group, IVB-NLCs (1.54 mg/kg) dose considerably delays the start of ST-segment depression (P 0.05) and significantly shortens its duration (P 0.05). IVB marketed tablets (1.54 mg/kg) initially produced significant effects on growth and decrease ST-segment depression period but only after the first day and statistically non-significant in disease control group.

Effect of ivabradine hydrochloride on the severity of ST-segment depression brought on by vasopressin: After the injection of vasopressin, IVB-NLCs (1.54 mg/kg) the ST-segment produced a substantial drop in height at 0, 1, 3, and 6 min, respectively. IBH pills that have been marketed have also resulted in notable shortages. When compared to the disease control group, the ST-segment only peaks for one day before declining again. Due to the ongoing release of the IBH-NLCs Property covered in the in-vitro part, there were three days of difficult activity.

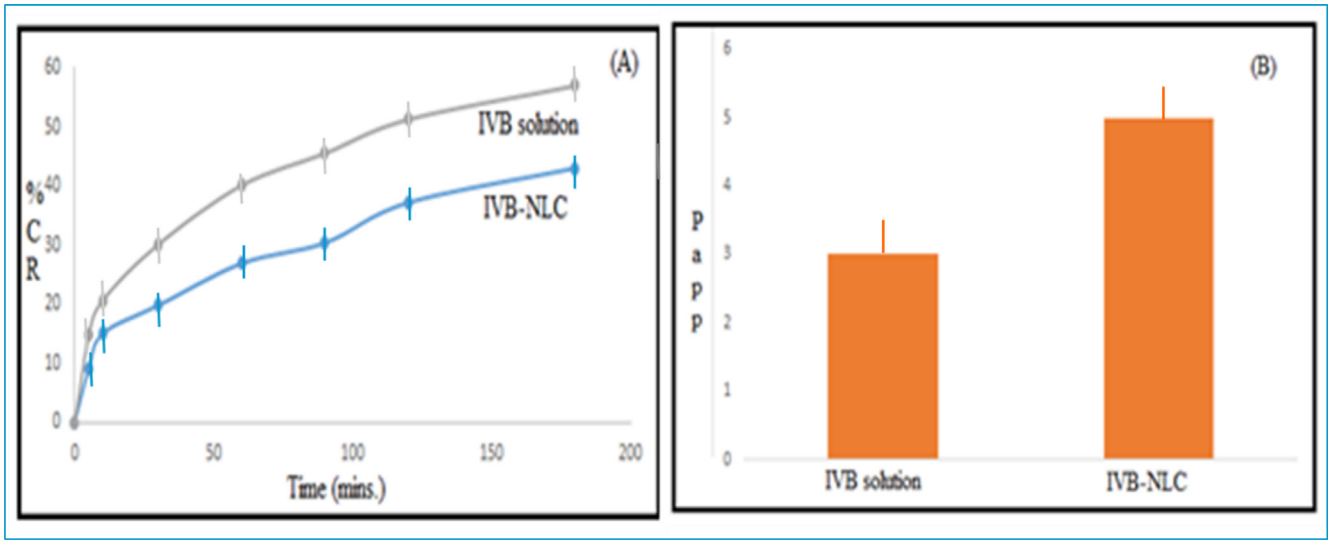

Fig. 6 (A) Ex-vivo permeation study of IVB solution and IVB-NLCs across rat intestinal membrane. (B) Apparent permeability coefficients (Papp) for IVB solution and IVB-NLCs.

5. Conclusion

The IVB-loaded NLCs were effectively prepared by high-pressure homogenization process using three-factor, three-level BBD optimization process produces seventeen-run. IVB-NLCs formulation was greatly influenced by the ratios of liquid to solid lipid and lecithin to poloxamer 188 since these variables affected the formulation's physical characteristics. The optimised IVB-NLCs manifested at 114. 45 ± 5. 14 nm in size and 83.45 ± 3.23% EE with distinct spherical globules of nanoscale size with a smooth surface were validated by TEM analysis. The change of IVB's crystalline character into an amorphous nature, which was confirmed by DSC and XRD, which is a key factor for improvement in absorption rate and enhancement of IVB bioavailability. Optimized batch have high permeability confirmed by ex-vivo study and The in-vivo pharmacological efficacy was demonstrated by a reduction in the intensity and duration of ST-segment depression in experimental rats with vasopressin-induced angina. The formulation is better compare to other marked formulation due to its high bioavailability and sustained release for longer duration.

Funding

This work was supported by Princess Nourah bint Abdulrahman University researchers supporting project number (PNURSP2023R205), Princess Nourah bint Abdulrahman University, Riyadh, Saudi Arabia. Also, it was supported by the Researchers Supporting Project number (RSPD2023R620), King Saud University, Riyadh, Saudi Arabia.

Institutional Review Board Statement: Not applicable.

Declaration of Competing Interest

The authors declare that they have no known competing financial interests or personal relationships that could have appeared to influence the work reported in this paper.

Acknowledgments

The authors extend their appreciation to the Researchers Supporting Project number (RSPD2023R620), King Saud University, Riyadh, Saudi Arabia. Also, the authors extend their appreciation to Princess Nourah bint Abdulrahman University, Riyadh, Saudi Arabia for funding this work under researcher supporting project number (PNURSP2023R205).

References

Ahmadian-Fard-Fini, S., Salavati-Niasari, M., Ghanbari, D., 2018. Hydrothermal green synthesis of magnetic Fe3O4-carbon dots by lemon and grape fruit extracts and as a photoluminescence sensor for detecting of E. coli bacteria. Spectrochim. Acta A Mol. Biomol. Spectrosc. 203, 481–493.

Ahmadian-Fard-Fini, S., Ghanbari, D., Salavati-Niasari, M., 2019. Photoluminescence carbon dot as a sensor for detecting of *Pseudomonas aeruginosa* bacteria: Hydrothermal synthesis of magnetic hollow $NiFe_2O_4$-carbon dots nanocomposite material. Compos. B Eng. 161, 564–577.

Ahmadian-Fard-Fini, S., Ghanbari, D., Amiri, O., Salavati-Niasari, M., 2020. Electro-spinning of cellulose acetate nanofibers/Fe/carbon dot as photoluminescence sensor for mercury (II) and lead (II) ions. Carbohydr. Polym. 229, 115428.

Ahmadian-Fard-Fini, S., Ghanbari, D., Amiri, O., Salavati-Niasari, M., 2021. Green sonochemistry assisted synthesis of hollow magnetic and photoluminescent $MgFe_2O_4$–carbon dot nanocomposite as a sensor for toxic Ni(II), Cd(II) and Hg(II) ions and bacteria. RSC Adv. 11 (37), 22805–22811.

Alagusundaram, M., Chengaiah, B., Ramkanth, S., Angala, P.S., Chetty, M., Dhachinamoorty, D., 2009. Formulation and evaluation of mucoadhesive buccal films of ranitidine. Int. J. Pharm. Tech. Res. 1, 557–563.

Braidy, N., Behzad, S., Habtemariam, S., Ahmed, T., Daglia, M., Nabavi, S.M., Sobarzo-Sanchez, E., Nabavi, S.F., 2017. Neuroprotective effects of citrus fruit-derived flavonoids, nobiletin and tangeretin in alzheimer's and parkinson's disease. C.N.S. Neurol. Disord. Drug Targets 16 (4), 387–397. https://doi.org/10.2174/1871527316666170328113309.

Deepika, D., Dewangan, H.K., Maurya, L., Singh, S., 2019. Intranasal drug delivery of frovatriptan succinate loaded polymeric nanoparticles for brain targeting. J. Pharm. Sci. 108 (2), 851–859. https://doi.org/10.1016/j.xphs.2018.07.013.

Dewangan, H.K., 2021. The emerging role of nanosuspensions for drug delivery and stability. CNANOM. 11 (4), 213–223. https://doi.org/10.2174/2468187312666211222123307.

Dewangan, H.K., Garg, A., 2020. A review: Application of nanotechnology for treatment of angina pectoris as cardiovascular disease. IJPSR 11 (10), 1000–1012.

Dewangan, H.K., Pandey, T., Maurya, L., Singh, S., 2018a. Rational design and evaluation of HBsAg polymeric nanoparticles as antigen delivery carriers. Int. J. Biol. Macromol. 111, 804–812. https://doi.org/10.1016/j.ijbiomac.2018.01.073.

Dewangan, H.K., Singh, S., Maurya, L., Srivastava, A., 2018b. Hepatitis B antigen loaded biodegradable polymeric nanoparticles: Formulation optimization and in-vivo immunization in BALB/C mice. Curr. Drug Deliv. 15 (8), 1204–1215. https://doi.org/10.2174/1567201815666180604110457.

Dewangan, H.K., Sharma, A., Mishra, A., Singour, P., 2021. Mucoadhesive microspheres of atorvastatin calcium: Rational design, evaluation and enhancement of bioavailability. Indian J. Pharm. Educ. Res. 55 (3s), S733–S741. https://doi.org/10.5530/ijper.55.3s.180.

Dewangan, H.K., Singh, N., Megh, S.K., Singh, S., Maurya, L., 2022. Optimization and evaluation of gymnema sylvestre (GYM) extract loaded polymeric nanoparticles for enhancement of in-vivo efficacy and reduction of toxicity. J. Microencapsul. 1–24.

Gandhi, A., Jana, S., Sen, K.K., 2014. In-vitro release of acyclovir loaded eudragit RLPO® nanoparticles for sustained drug delivery. Int. J. Biol. Macromol. 67, 478–482. https://doi.org/10.1016/j.ijbiomac.2014.04.019.

Hirata, Y., Mabuchi, H.M., Sasaki, T., Maruyama, H., Kase, Y., Takeda, S., Aburada, M., 2005. Antianginal effects of lercanidipine or methacholine on the vasopressin induced angina model in rats. Biol. Pharm. Bull. 28, 811–816.

Hung, L.M., Su, M.J., Chen, J.K., 2004. Resveratrol Protects Myocardial- Ischemia-Reperfusion Injury Through Both NO-Dependent and NO− Independent Mechanisms. Free Radic. Biol. Med. 36 (6), 774–781. https://doi.org/10.1016/j.freeradbiomed.2003.12.016.

Ikeda, J., Matsubara, M., Yao, K., 2006. Effects of benidipine in a rat model for experimental angina. Yakugaku Zasshi 126 (12), 1377–1381. https://doi.org/10.1248/yakushi.126.1377.

Joshi, M.D., Müller, R.H., 2009. Lipid Nanoparticles for Parenteral Delivery of Actives. Eur. J. Pharm. Biopharm. 71 (2), 161–172. https://doi.org/10.1016/j.ejpb.2008.09.003.

Karami, M., Ghanbari, M., Alshamsi, H.A., Rashki, S., Salavati-Niasari, S., 2021. Facile fabrication of Tl 4 HgI 6 nanostructures as novel antibacterial and antibiofilm agents and photocatalysts in the degradation of organic pollutants. Inorg. Chem. Front. 8 (10), 2442–2460.

Kavousi, F., Goodarzi, M., Ghanbari, D., Hedayati, K., 2019. Synthesis and characterization of a magnetic polymer nanocom-

posite for the release of metoprolol and aspirin. J. Mol. Struct. 1183, 324–330.

Lakshmi, S.K. and Dewangan, H. K. 2022. Dual vinorelbine bitartrate and resveratrol loaded polymeric aqueous core nanocapsules for synergistic efficacy in breast cancer. J. Microencapsul. 1–15 (IF: 3.2). DOI: 10.1080/02652048.2022.2070679.

Lakshmi, S.S., Singh, S., Vijayakumar, M.R., Dewangan, H.K., 2018. Lipid based aqueous core nanocapsules (acns) for encapsulating hydrophilic vinorelbine bitartrate: Preparation, optimization, characterization and in vitro safety assessment for intravenous administration. Curr. Drug Deliv. 15 (9), 1284–1293. https://doi.org/10.2174/1567201815666180716112457.

Mishra, A.K., Neha, S.L., Rani, L., Dewangan, H.K., Sahoo, P.K., 2023a. QbD assisted development and validation of UV spectroscopic method in estimation of silymarin. Lett Drug Des Discov., 20

Mishra, A.K., Neha, S.L., Rani, L., Jain, A., Dewangan, H.K., Sahoo, P.K., 2023b. Rationally designed nanoparticulate delivery approach for silymarin with natural bio-enhancer: *in vitro* characterization and in vivo evaluations of hepatoprotective effects in a mouse model. J Drug Deliv Sci Technol. 86,. https://doi.org/10.1016/j.jddst.2023.104580 104580.

Müller, R.H., Radtke, M., Wissing, S.A., 2002. Nanostructured lipid matrices for improved microencapsulation of drugs. Int. J. Pharm. 242 (1–2), 121–128. https://doi.org/10.1016/s0378-5173(02)00180-1.

Müller, R.H., Petersen, R.D., Hommoss, A., Pardeike, J., 2007. Nanostructured lipid carriers (NLC) in cosmetic dermal products. Adv. Drug Deliv. Rev. 59 (6), 522–530. https://doi.org/10.1016/j.addr.2007.04.012.

Ngan, C.L., Basri, M., Lye, F.F., Fard Masoumi, H.R., Tripathy, M., Abedi Karjiban, R., Abdul-Malek, E., 2014. Comparison of box-behnken and central composite designs in optimization of fullerene loaded palm-based nano-emulsions for cosmeceutical application. Ind. Crops Prod. 59, 309–317. https://doi.org/10.1016/j.indcrop.2014.05.042.

O'Driscoll, C.M., Griffin, B.T., 2008. Biopharmaceutical challenges associated with drugs with low aqueous solubility—the potential impact of lipid-based formulations. Adv. Drug Deliv. Rev. 60 (6), 617–624. https://doi.org/10.1016/j.addr.2007.10.012.

Onoue, S., Uchida, A., Takahashi, H., Seto, Y., Kawabata, Y., Ogawa, K., Yuminoki, K., Hashimoto, N., Yamada, S., 2011. Development of highenergy amorphous solid dispersion of nano-sized nobiletin, a citrus polymethoxylated flavone, with improved oral bioavailability. J. Pharm. Sci. 100 (9), 3793–3801. https://doi.org/10.1002/jps.22585.

Orooji, Y., Ghanbari, M., Amiri, O., Salavati-Niasari, M., 2020. Facile fabrication of silver iodide/graphitic carbon nitride nanocomposites by notable photo-catalytic performance through sunlight and antimicrobial activity. J. Hazardous Materials. 389, 122079.

Pradhan, M., Singh, D., Murthy, S.N., Singh, M.R., 2015. Design, characterization and skin permeating potential of fluocinolone acetonide loaded nanostructured lipid carriers for topical treatment of psoriasis. Steroids 101, 56–63. https://doi.org/10.1016/j.steroids.2015.05.012.

Raghuvanshi, A., Shah, K., Dewangan, H.K., 2022. Ethosome as antigen delivery carrier: optimization, evaluation and induction of immunological response via nasal route against hepatitis B. J. Microencapsul. 28, 1–24.

Sharma, V., Dewangan, H.K., Maurya, L., Vats, K., Verma, H., Singh, S., 2019. Rational design and in-vivo estimation of ivabradine hydrochloride loaded nanoparticles for management of stable angina. J. Drug Deliv. Sci. Technol. 54, 43–54. https://doi.org/10.1016/j.jddst.2019.101337.

Sharma, A.N., Upadhyay, P.K., Dewangan, H.K., 2022. Development, evaluation, pharmacokinetic and biodistribution estimation of resveratrol-loaded solid lipid nanoparticles for prostate cancer targeting. J. Microencapsul. 39 (6), 563–574. https://doi.org/10.1080/02652048.2022.2135785.

Singh, S.K., Dadhania, P., Vuddanda, P.R., Jain, A., Velaga, S., Singh, S., 2016. Intranasal delivery of asenapine loaded nanostructured lipid carriers: Formulation, characterization, pharmacokinetic and behavioural assessment. R.S.C. Adv. 6 (3), 2032–2045. https://doi.org/10.1039/C5RA19793G.

Singh, S., Dobhal, A.K., Jain, A., Pandit, J.K., Chakraborty, S., 2010. Formulation and evaluation of solid lipid nanoparticles of a water soluble drug: Zidovudine. Pharmceutical bulletin. Chem. Pharm. Bull. (Tokyo) 58 (5), 650–655. https://doi.org/10.1248/cpb.58.650.

Sun, M., Nie, S., Pan, X., Zhang, R., Fan, Z., Wang, S., 2014. Quercetin- nanostructured lipid carriers: characteristics and anti-breast cancer activities in vitro. Colloids Surf. B Biointerfaces 113, 15–24. https://doi.org/10.1016/j.colsurfb.2013.08.032.

Yadav, D., Semwal, B.C., Dewangan, H.K., 2022a. Grafting, characterization and enhancement of therapeutic activity of berberine loaded pegylated PAMAM dendrimer for cancerous cell. J. Biomater. Sci. Polym. Ed. 14, 1–14. https://doi.org/10.1080/09205063.2022.2155782.

Yadav, R.K., Shah, K., Dewangan, H.K., 2022b. Intranasal drug delivery of sumatriptan succinate loaded polymeric solid lipid nanoparticles for brain targeting. Drug Dev. Ind. Pharm. 15, 1–22. https://doi.org/10.1080/03639045.2022.2090575.

Ye, Z., Wang, W., Yuan, Q., Ye, H., Sun, Y., Zhang, H., Zeng, X., 2016. Box-behnken design for extraction optimization, characterization and in vitro antioxidant activity of Cicer arietinum L. Hull polysaccharides. Carbohydr. Polym. 147, 354–364. https://doi.org/10.1016/j.carbpol.2016.03.092.